Kernel Synthesis for Generalized Time–Frequency Distributions Using the Method of Alternating Projections Onto Convex Sets

Seho Oh, Robert J. Marks, II, *Fellow, IEEE,* and Les E. Atlas

***Abstract*— Cohen's generalized time–frequency distribution (GTFR) requires the choice of a two-dimensional kernel. The kernel directly affects many performance attributes of the GTFR such as time resolution, frequency resolution, realness, and conformity to time and frequency marginals. A number of different kernels may suffice for a given performance constraint (high-frequency resolution, for example). Interestingly, most sets of kernels satisfying commonly used performance constraints are convex. In this paper, we describe a method whereby kernels can be designed that satisfy two or more of these constraints. If there exists a nonempty intersection among the constraint sets, then the theory of *alternating projection onto convex sets* (POCS) guarantees convergence to a kernel that satisfies all of the constraints. If the constraints can be partitioned into two sets, each with a nonempty intersection, then POCS guarantees convergence to a kernel that satisfies the inconsistent constraints with minimum mean-square error. We apply kernels synthesized using POCS to the generation of some example GTFR's, and compare their performance to the spectrogram, Wigner distribution, and cone kernel GTFR.**

I. Introduction

THERE are many applications for time–frequency representations (TFR's). The most commonly used TFR is the spectrogram [1]. Other approaches include wavelets [2] and generalized time–frequency representations (GTFR's) [5]. With a spectrogram, a window is chosen in accordance with desired performance properties, most commonly, a time resolution versus frequency resolution tradeoff. Similarly, the GTFR requires a kernel that is chosen in accordance with desired performance attributes. Good time resolution, for example, is achieved when the two-dimensional kernel is zero outside a cone [9], [10]. The requirement that a GTFR exhibits proper temporal and frequency marginals can also be translated to structural constraints on the kernel. The set of all kernels satisfying the frequency marginals is convex. The set of all cone kernels also is convex. Remarkably, most other commonly used GTFR performance constraints, when imposed on the kernel, result in a convex set of permissible kernels. Finding a kernel that satisfies two or more constraints then is equivalent to finding a point in the intersection of the corresponding (convex) constraint sets.

An open issue is whether a given kernel exists which satisfies, or approximately satisfies, two or more constraints simultaneously. This paper shows how the technique of alternating projections onto convex sets (POCS) can be used to synthesize kernels which satisfy multiple constraints. We empirically prove that a kernel satisfying all commonly used performance attributes does not exist. A kernel designed on a subset of desired performance attributes is shown to perform superiorly to some other commonly used fixed kernel GTFR's.

Manuscript received April 15, 1991; revised May 4, 1993. This work was supported in part by the Washington Technology Center. The associate editor coordinating the review of this paper and approving it for publication was Prof. Miguel A. Lagunas.

S. Oh was with the Department of Electrical Engineering, University of Washington, Seattle, WA 98195. He is now with Neopath Inc., Seattle, WA, USA.

R. J. Marks, II and L. E. Atlas are with the Interactive Systems Design Laboratory, Department of Electrical Engineering, University of Washington, Seattle, WA 98195 USA.

IEEE Log Number 9401251.

II. Preliminaries

The generalized time–frequency representation (GTFR) of a temporal signal $x(t)$ can be written as [4], [5]

$$C(t,u) = \int_{-\infty}^{\infty}\int_{-\infty}^{\infty} \hat{\phi}(t-\xi,\tau)x\left(\xi+\frac{\tau}{2}\right) \cdot x^*\left(\xi-\frac{\tau}{2}\right)e^{-j2\pi u\tau}\,d\xi d\tau \tag{1}$$

where $\hat{\phi}(t,\tau)$ is the kernel of the GTFR and u is the frequency variable. The specific choice of the kernel dictates the performance of the GTFR. Typically, constraints are placed on the kernel in order to enhance various characteristics of the GTFR [3]–[10].

In order to facilitate discussion, we define the following Fourier transforms on the kernel:

$$\phi(f,\tau) = \int_{-\infty}^{\infty} \hat{\phi}(t,\tau)e^{-j2\pi ft}\,dt,$$

$$\hat{\Phi}(t,u) = \int_{-\infty}^{\infty} \hat{\phi}(t,\tau)e^{-j2\pi u\tau}\,d\tau,$$

and

$$\Phi(f,u) = \int_{-\infty}^{\infty}\int_{-\infty}^{\infty} \hat{\phi}(t,\tau)e^{-j2\pi(u\tau+ft)}\,dt\,d\tau.$$

The various transforms of the kernel are summarized in Table I.

TABLE I
KERNEL FOR COHEN'S GTFR EXPRESSED IN VARIOUS FOURIER TRANSFORM DOMAINS. EACH A RROW CORRESPONDS TO A 1-D FOURIER TRANSFORM

t	f
τ $\hat{\phi}(t,\tau) \rightarrow$	$\phi(f,\tau)$
$\downarrow$	$\downarrow$
u $\hat{\Phi}(t,u) \rightarrow$	$\Phi(f,u)$

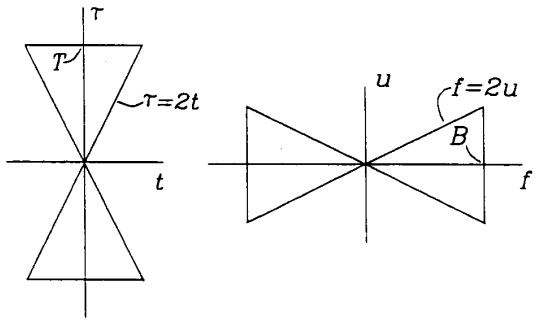

Fig. 1. Cone and bow-tie constraints. On the (t,τ) plane shown in (a), the kernel $\hat{\phi}(t,\tau)$ is zero outside the cone shown if it is to obey the time resolution constraint. The set of all such functions obeying this constraint is convex. The dual frequency resolution constraint requires $\Phi(f,u)$ to be zero outside the bow tie shown in (b). The set of all functions obeying this constraint is also convex.

III. KERNEL CONSTRAINTS

Using the kernels summarized in Table I, we can straightforwardly state some of the commonly used constraints imposed on the GTFR and their corresponding interpretation as kernel constraints.

1) Time Resolution Constraint: As is illustrated in Fig. 1(a), the requirement that the input $x(t)$ on the interval $-T \leq t-\xi \leq T$ only contribute to the GTFR at time $t-\xi$ is achieved when the kernel is zero outside a cone [5], [9]. In other words,

$$\hat{\phi}(t,\tau) = \hat{\phi}(t,\tau)\Pi\left(\frac{t}{\tau}\right)\Pi\left(\frac{\tau}{2T}\right) \tag{2}$$

where the rectangle function $\Pi(t)$ is one for $|t| \leq \frac{1}{2}$ and is zero otherwise.

2) Interference Suppression Constraint: The magnitude of the interference at frequency f between two tones at frequencies f_1 and f_2 is zero when

$$\Phi\left(f_1 - f_2, f - \frac{f_1+f_2}{2}\right) = 0. \tag{3}$$

This equation results by using the signal $x(t) = \exp(j2\pi f_1 t) + \exp(j2\pi f_2 t)$ in (1). This constraint is met if

$$\Phi(f,u) = \Theta(u)\delta(f)$$

where $\Theta(u)$ is an arbitrary one-dimensional function and $\delta(f)$ is the Dirac delta impulse. This constraint, also discussed by Loughlin *et al.* [11], is equivalent to requiring that

$$\hat{\phi}(t,\tau) = \theta(\tau). \tag{4}$$

A relaxed interference constraint is

$$\Phi(f,u) = \Phi(f,u)\Pi\left(\frac{f}{2\Delta}\right) \tag{5}$$

where Δ, with units of frequency, can be thought of as an *interference bandwidth.* If $\Delta = 0$, there is no interference.

3) Frequency Resolution Constraint: The GTFR in (1) can also be written as

$$C(t,u) = \int_{-\infty}^{\infty}\int_{-\infty}^{\infty} \Phi(f,u-\nu)X\left(\nu+\frac{f}{2}\right) \cdot X^*\left(\nu-\frac{f}{2}\right)e^{j2\pi ft}\,d\nu\,df. \tag{6}$$

Comparing with (1) immediately suggests a frequency resolution constraint that is the dual of the cone constraint in (2):

$$\Phi(f,u) = \Phi(f,u)\Pi\left(\frac{f}{u}\right)\Pi\left(\frac{f}{2B}\right) \tag{7}$$

where the bandwidth B is the frequency dual of T.

For finite B and T, the constraints in (2) and (7) cannot be satisfied simultaneously. We are therefore motivated to formulate the following relaxed version of (7). The kernel is constrained to satisfy the bound

$$0 \leq \Phi(f,u) \leq \alpha(f,u) \tag{8}$$

where $\alpha(f,u)$ is a given positive function such as

$$\alpha(f,u) = \alpha(0,0)\exp(-\beta|f| + \gamma|u|) \tag{9}$$

and β and γ are given constants. The bandwidth B can here be interpreted as the 3 dB point from the maximum ($B = \ln 2/\beta$). Note, also, that the interference constraint in (5) can be imposed by the bound in (8), possibly in a relaxed form. Positive functions other than the exponentials in (9) can also be used. We found this bound to give good results.

4) Frequency Marginal Constraint [3]: Define the power spectral density of a signal $x(t)$ by

$$P(u) = \int_{-\infty}^{\infty} R(\tau)e^{-j2\pi u\tau}\,d\tau \tag{10}$$

where the autocorrelation of the signal is

$$R(\tau) = \int_{-\infty}^{\infty} x\left(\xi+\frac{\tau}{2}\right)x^*\left(\xi-\frac{\tau}{2}\right)d\xi.$$

A desirable property of a GTFR is the frequency marginal constraint

$$P(u) = \int_{-\infty}^{\infty} C(t,u)\,dt.$$

This is clearly achieved if

$$\int_{-\infty}^{\infty} \hat{\phi}(t,\tau)\,dt = 1 \tag{11}$$

and is equivalent to requiring that

$$\phi(0,\tau) = 1. \tag{12}$$

5) Time Marginal Constraint [3]: Similar to the previous frequency marginal, we desire to have an instantaneous power marginal:

$$|x(t)|^2 = \int_{-\infty}^{\infty} C(t,u)\,du.$$

This is achieved when

$$\phi(f,0) = 1. \tag{13}$$

6) Realness Constraint: A sufficient condition for $C(t,u)$ to be real is that the kernel be conjugately symmetric:

$$\phi(f,\tau) = \phi^*(-f,-\tau). \tag{14}$$

This is equivalent to requiring that $\hat{\Phi}(t,u)$ be real:

$$\mathcal{R}\hat{\Phi}(t,u) = \hat{\Phi}(t,u) \tag{15}$$

where $\mathcal{R}$ denotes *the real part of.*

7) Time Symmetry Constraint: At a given point temporal point, past and future time are treated symmetrically if

$$\phi(f,\tau) = \phi^*(f,-\tau). \tag{16}$$

Note that, assuming differentiability, it follows that

$$\left.\frac{\partial\phi(f,\tau)}{\partial\tau}\right|_{\tau=0} = 0.$$

This and (13) constitute the *instantaneous frequency* constraint [3].

8) Frequency Symmetry Constraint: Similarly, for frequency symmetry, we impose the constraint

$$\phi(f,\tau) = \phi^*(-f,\tau). \tag{17}$$

Again, assuming differentiability, this requires that

$$\left.\frac{\partial\phi(f,\tau)}{\partial f}\right|_{f=0} = 0. \tag{18}$$

Note that imposition of any two of the previous three constraints imposes the third. Equations (18) and (12) constitute the *group delay* constraint [3].

9) Nonnegativity Constraint: We may wish to require that

$$\hat{\phi}(t,\tau) = \mathcal{R}\hat{\phi}(-t,\tau)\mu[\mathcal{R}\hat{\phi}(-t,\tau)] \tag{19}$$

where $\mu(\cdot)$ is the unit step. In other words, the real part of $\hat{\phi}(t,\tau)$ is nonnegative.

10) Finite Area Constraint: A constraint that is useful in the iterative synthesis procedure to be described later in this paper is

$$\Phi(0,0) = \gamma > 0 \tag{20}$$

or, equivalently,

$$\int\int \hat{\phi}(t,\tau)\,dt\,d\tau = \gamma.$$

This constraint can prohibit the projection onto convex sets iteration from converging to the degenerate result that the kernel is everywhere identically equal to zero.

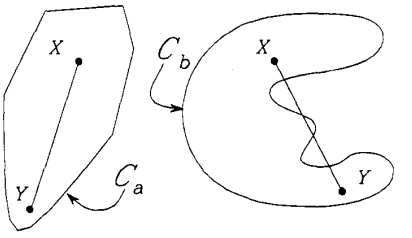

Fig. 2. Set C_a on the left is convex. All line segments with endpoints X and Y within the set are totally subsumed within the set. The set C_b on the right is clearly not convex, as illustrated by the counterexample shown.

IV. POCS

All of the constraints in the previous section are convex in the sense that, if the kernels ϕ_1 and ϕ_2 satisfy any one given constraint, then for any α in the interval $0 \le \alpha \le 1$, the kernel $\alpha\phi_1 + (1-\alpha)\phi_2$ satisfies the same constraint. For example, if ϕ_1 and ϕ_2 obey the cone constraint, then so does $\alpha\phi_1 + (1-\alpha)\phi_2$. If ϕ_1 and ϕ_2 obey the frequency marginal constraint, then so does $\alpha\phi_1 + (1-\alpha)\phi_2$, etc. The convexity of the constraints allows the use of the powerful synthesis procedure of *alternating projection onto convex sets* (POCS).[1] POCS was initially introduced by Bregman [12] and Gubin *et al.* [13], and was later popularized by Youla and Webb [14] and Sezan and Stark [15]. POCS has been applied to such topics as sampling theory [16], fuzzy set theory [17], and artificial neural networks [18], [19]. The synthesis of GTFR kernels using POCS described in this paper parallels the synthesis of windows proposed by Goldburg and Marks [20]. A superb overview of POCS with other applications is in the book by Stark [21].

We now present an abbreviated introduction to POCS.

A. Convex Sets

Let $\mathcal{C}$ denote a set of functions. The set $\mathcal{C}$ is said to be convex if, for every $X \in \mathcal{C}$ and $Y \in \mathcal{C}$,

$$\alpha X + (1-\alpha)Y \in \mathcal{C}; \qquad 0 \le \alpha \le 1.$$

Geometrically, this is interpreted as shown in Fig. 2. A set is convex if, for every two points chosen within the set, all of the points in the line segment connecting the two points are also in the set. The set on the left in Fig. 2 is convex. Geometrical shapes corresponding to convex sets include balls, line segments, planes, boxes, and quadrants. The set shown on the right in Fig. 2 is clearly not convex.

B. Convex Set Projections

The *projection* of an arbitrary function Z onto a (compact) convex set $\mathcal{C}$ is the unique function in $\mathcal{C}$ that is closest to Z in the mean-square sense. This is geometrically illustrated in Fig. 3. Denote the projection operator by $\mathcal{P}_{\mathcal{C}}$ and the projection by $\mathcal{P}_{\mathcal{C}}Z$. Note that, if $Z \in \mathcal{C}$, then $\mathcal{P}_{\mathcal{C}}Z = Z$. In other words, if a function is already within the set, then the projection is an identity operation. It follows that $\mathcal{P}_{\mathcal{C}}^2 = \mathcal{P}_{\mathcal{C}}$.

[1] The *alternating* term is implicit in the POCS paradigm, but traditionally not included in the acronym.

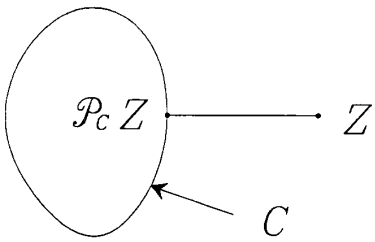

Fig. 3. As illustrated here, the projection of a function Z onto the convex set C is that unique point in C that is closest to Z in the mean-square sense. The result of the projection is the point $\mathcal{P}_C Z$.

TABLE II
SUMMARY OF THE CONVEX SETS AND THEIR PROJECTIONS OF COHEN'S CLASS KERNEL

Convex Set	Equation Number	Projection
$\mathcal{C}_1$	(2)	$\hat{\phi}(t,\tau)\times\Pi\left(\frac{t}{\tau}\right)\Pi\left(\frac{\tau}{2T}\right)$
$\mathcal{C}_2$	(5)	$\Phi(f,u)\times\Pi\left(\frac{f}{2\Delta}\right)$
$\mathcal{C}_{3,1}$	(7)	$\Phi(f,u)\times\Pi\left(\frac{f}{u}\right)\Pi\left(\frac{f}{2B}\right)$
$\mathcal{C}_{3,2}$	(8)	$0;\quad \Phi(f,u)\le 0$ $\Phi(f,u);\quad 0<\Phi(f,u)\le\alpha(f,u)$ $\alpha(f,u);\quad \Phi(f,u)>\alpha(f,u)$
$\mathcal{C}_4$	(12)	$\phi(0,\tau)=1$
$\mathcal{C}_5$	(13)	$\phi(f,0)=1$
$\mathcal{C}_6$	(14)	$[\phi(f,\tau)+\phi^*(-f,-\tau)]/2$
$\mathcal{C}_7$	(16)	$[\phi(f,\tau)+\phi^*(f,-\tau)]/2$
$\mathcal{C}_8$	(17)	$[\phi(f,\tau)+\phi^*(-f,\tau)]/2$
$\mathcal{C}_9$	(19)	$\hat{\phi}(t,\tau)\times\mu[\hat{\phi}(t,\tau)]$
$\mathcal{C}_{10}$	(20)	$\Phi(0,0)=\gamma$

We illustrate with sample projection operators from the convex constraints of the kernels in the previous section. A summary of convex sets and corresponding projections is shown in Table II. A more extensive list of projection operators can be found in Youla and Webb's paper [14] and in Stark's book [21]. In the examples here, we will use the form of the kernel in Table I that most easily explains the projection. Any of the four choices of domains can be accessed from any other by the appropriate Fourier transform. Inherent in the projection notation is the assumption that the kernel is in the proper domain.

1) Time and Frequency Resolution Projections: For time resolution (Constraint 1)), the signal outside the cone on the (t,τ) plane is simply set to zero:

$$\mathcal{P}_{\mathcal{C}_1}\hat{\phi}(t,\tau)=\hat{\phi}(t,\tau)\Pi\left(\frac{t}{\tau}\right)\Pi\left(\frac{\tau}{2T}\right).$$

Similarly, for frequency resolution constraint 3), the area outside the bow tie on the (f,u) plane is set to zero:

$$\mathcal{P}_{\mathcal{C}_{3,1}}\Phi(f,u)=\Phi(f;u)\Pi\left(\frac{f}{u}\right)\Pi\left(\frac{f}{2B}\right). \tag{21}$$

The relaxed version of frequency resolution is

$$\mathcal{P}_{\mathcal{C}_{3,2}}\Phi(f,u)=\begin{cases}0; & \Phi(f,u)<0\\ \Phi(f,u); & 0\le\Phi(f,u)\le\alpha(f,u)\\ \alpha(f,u); & \Phi(f,u)>\alpha(f,u).\end{cases}$$

2) Realness and Symmetry Constraint: The realness constraint 6) can be imposed by the projection operator

$$\mathcal{P}_{\mathcal{C}_6}\hat{\Phi}(t,u)=\mathcal{R}\hat{\Phi}(t,u)$$

or, equivalently, in the (f,τ) plane,

$$\mathcal{P}_{\mathcal{C}_6}\phi(f,\tau)=\tfrac{1}{2}[\phi(f,\tau)+\phi^*(-f,-\tau)].$$

Similarly, for the symmetry constraints in (16) and (17), the respective projection operators can be written as

$$\mathcal{P}_{\mathcal{C}_7}\phi(f,\tau)=\tfrac{1}{2}[\phi(f,\tau)+\phi^*(f,-\tau)]$$

and

$$\mathcal{P}_{\mathcal{C}_8}\phi(f,\tau)=\tfrac{1}{2}[\phi(f,\tau)+\phi^*(-f,\tau)]. \tag{22}$$

3) Relaxed Interference Projection: Motivated by (5), the projection operator corresponding to the relaxed interference term in constraint 3) is

$$\mathcal{P}_{\mathcal{C}_2}\Phi(f,u)=\Phi(f,u)\Pi\left(\frac{f}{2\Delta}\right).$$

Note that if Δ is large enough and B is small enough, the frequency resolution projection in (21) subsumes this projection.

4) Nonnegative Projection: The nonnegativity constraint can be inposed by the projection

$$\mathcal{P}_{\mathcal{C}_9}\hat{\phi}(t,\tau)=\hat{\phi}(t,\tau)\mu[\hat{\phi}(t,\tau)].$$

5) Marginal and Cone Constraint: In some cases, projections can be best described by the intersection of two or more convex constraints. Combining the time resolution constraint and the frequency marginal constraint in (10), we can write the projection on the intersection of the three sets as the convex set operator

$$\mathcal{P}_{\mathcal{C}_1\cap\mathcal{C}_4\cap\mathcal{C}_5}\hat{\phi}(t,\tau)=\begin{cases}\delta(t);\tau=0\\ [\hat{\phi}(t,\tau)+\varphi(\tau)]\Pi\left(\frac{t}{\tau}\right)\Pi\left(\frac{\tau}{2T}\right);\\ \text{otherwise}\end{cases}$$

where $\cap$ denotes intersection, $\delta(\cdot)$ is the Dirac delta function, and

$$\varphi(\tau)=\frac{1}{|\tau|}\left[1-\int_{-|\tau|/2}^{|\tau|/2}\hat{\phi}(t,\tau)\,dt\right].$$

Combining the time resolution and the finite area constraints, we have the projection

$$\mathcal{P}_{\mathcal{C}_1\cap\mathcal{C}_{10}}\hat{\phi}(t,\tau)=[\hat{\phi}(t,\tau)+\varphi]\Pi\left(\frac{t}{\tau}\right)\Pi\left(\frac{\tau}{2T}\right)$$

where

$$\varphi=\frac{1}{T^2}\left[1-\int_{\tau=-T}^{T}\int_{t=-(|\tau|/2)}^{|\tau|/2}\hat{\phi}(t,\tau)\,dt\,d\tau\right].$$

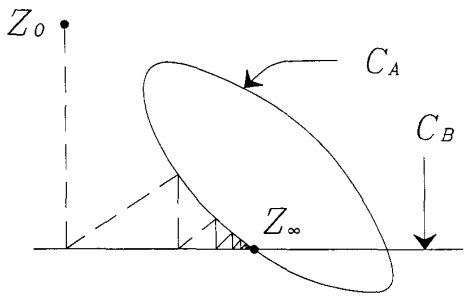

Fig. 4. Alternating projection between two intersecting convex sets C_A and C_B iteratively approaches a fixed point Z_∞ common to both sets. If there is more that one point in the intersection, the fixed point will be a function of the initialization of the interation that, in this example, is Z_0.

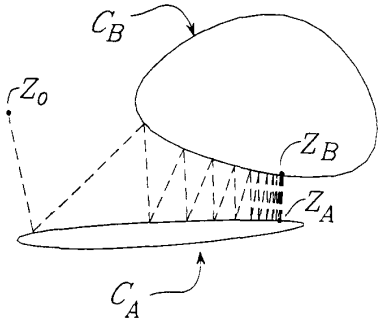

Fig. 5. Alternating projection between two nonintersecting convex sets C_A and C_B iteratively approaches a limit cycle between two points in each set. In this illustration, these points are Z_A and Z_B. Note that Z_A is the point in C_A that is closest to C_B and vice versa. The solution is thus a minimum mean-square error solution. Although it is not always the case, the limit cycle here is independent of initialization Z_0. If there exists more than one possible limit cycle, each will have points separated by the same distance.

C. Alternating Projections

There are three fundamental lemmas in the theory of POCS. We will state each lemma and illustrate it geometrically.[2]

Lemma 1: Alternately projecting between two or more convex sets with a nonempty intersection will iteratively converge to a point common to all sets [14], [21].

This is illustrated in Fig. 4. Note that the point of convergence generally depends on the initialization. If, however, there is a single point of intersection (e.g., two lines), then convergence will be independent of the initialization.

Lemma 2: Alternately projecting between two nonintersecting convex sets will converge to a limit cycle between points in each set closest to the other set [20].

This is illustrated in Fig. 5. This property can be used to find the best member in a set that is closest to another set in the mean-square sense. Note that, as can be visualized in the case of two parallel line convex sets, the limit cycle is not unique.

This property generalizes to more than three sets in the following sense. Let two or more constraints have a nonempty intersection C_a. Let two or more other constraints have a nonempty intersection C_b. If C_a and C_b do not intersect, then POCS will converge to a limit cycle between points convex sets C_a and C_b, each closest to the other in the mean-square sense.

[2]For continuous variable functions, POCS converges, at worst, weakly. POCS applied to discrete-time signals, however, always displays strong convergence.

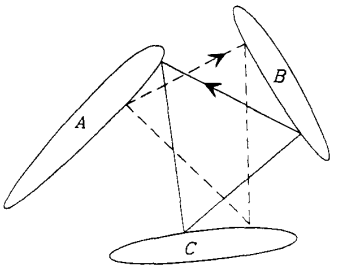

Fig. 6. A number of different limit cycles can exist when three or more convex sets do not intersect. Here, projecting from set A to B to C gives a different limit cycle than projecting them in reverse order.

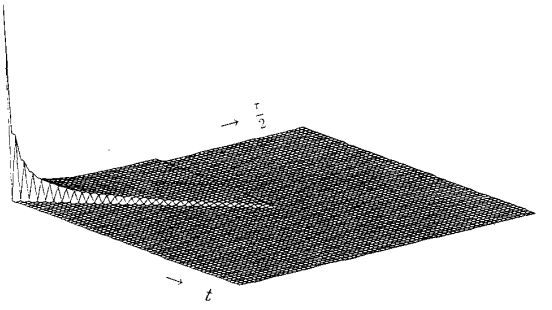

Fig. 7. One quadrant of the symmetric cone kernel in the (t, τ) plane synthesized using all the POCS constraints listed in this paper. The iteration reached a limit cycle. Thus, all of the constraints could not be simultaneously met for finite T and B.

Lemma 3: Alternately projecting between three or more nonintersecting convex sets will result in a limit cycle that can be dependent on both the ordering of the projections and the initialization [22].

This final lemma states, unfortunately, that POCS can yield results for questionable worth when three or more of the convex sets do not intersect. Two different limit cycles corresponding to different orderings of the projection are geometrically illustrated in Fig. 6 for the case of three nonintersecting sets.

V. POCS Kernel Synthesis

The use of POCS in the design of GTFR kernels is now evident. We choose from a menu of convex constraints that we desire our GTFR to obey. By alternately projecting between the corresponding convex sets, we hope to synthesize a corresponding kernel. If the convex sets meet the suppositions of Lemma 1, a kernel meeting all constraints will be generated. If the constraints in Lemma 2 are met, we will be guaranteed that the constraints have been met in a mean-square sense. This may or may not be acceptable, depending on the magnitude of the mean-square error. Note, however, that this is a problem of the problem rather than that of the synthesis method. In

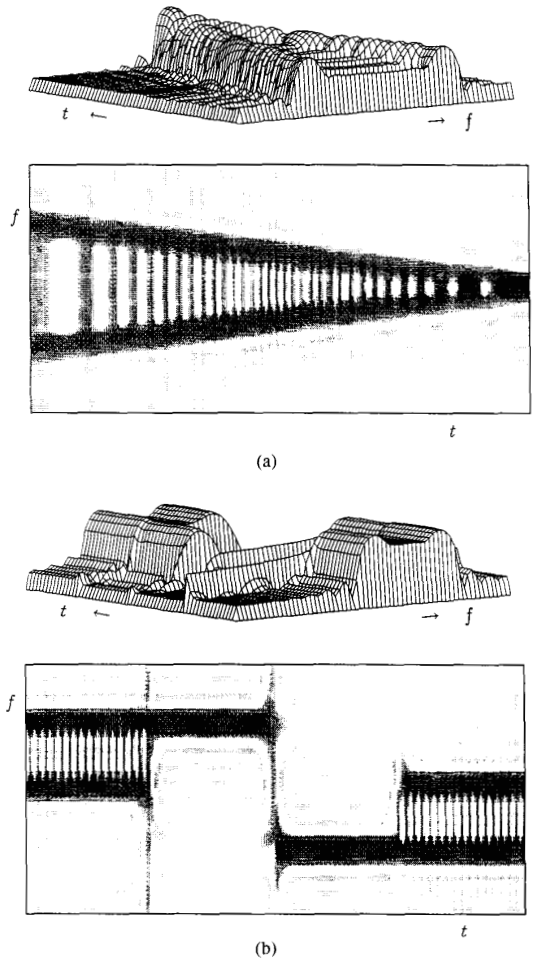

Fig. 8. Waterfall and gray-level display of two linearly converging chirps (a) and two-tone signal with transition (b) using the POCS-designed kernel in Fig. 7. There is significant smoothing between the tones.

other words, the distances between the constraint sets are too large to allow for any acceptable solution.

To illustrate the potential use of POCS in kernel design, we present two preliminary examples. Both examples were computed on a 128×128 grid. The kernels in both examples are both the cone and bow-tie constraints. The value of T in each case corresponded to truncating the grid so that the cone had a peak-to-peak height of 64. Both examples resulted in a kernel that was positive and symmetric.

Example 1 used, in addition, both marginal constraints. We take the alternating projection between the set $\mathcal{C}_{3,1} \cap \mathcal{C}_{3,2}$ and $\mathcal{C}_1 \cap \mathcal{C}_4 \cap \mathcal{C}_5 \cap \mathcal{C}_9$. The resulting kernel is pictured in Fig. 7. It resembles a truncated Born–Jordan [4] kernel which has a $1/|\tau|$ taper within the cone. Indeed, for $B = \infty$ and $T = \infty$, the Born–Jordan kernel satisfies all the constraints. Specifically,

$$\hat{\phi}(t,\tau) = \frac{1}{|\tau|}\Pi\left(\frac{t}{\tau}\right)$$

satisfies the cone constraint in (2). Furthermore, the marginal constraints in (11) and (13) are met, as are the symmetry

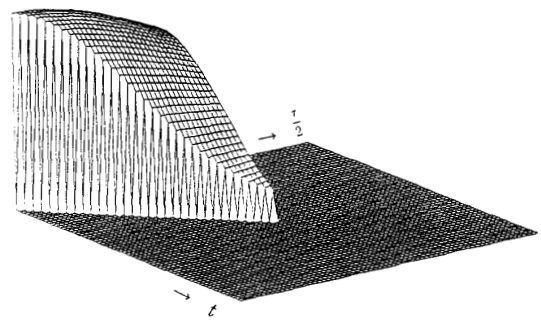

Fig. 9. One quadrant of the symmetric cone kernel on the (t, τ) plane synthesized using all the POCS constraints listed in this paper except the power spectral density and instantaneous power marginals.

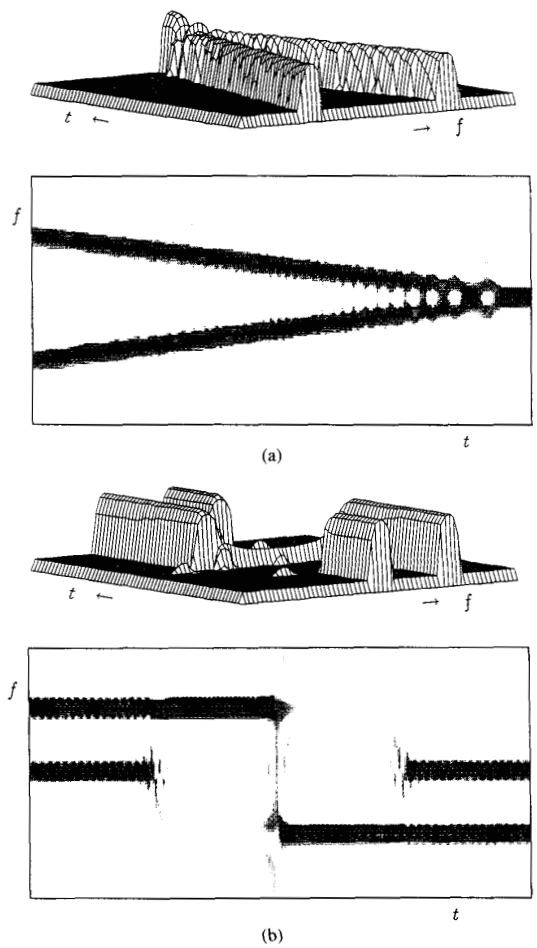

Fig. 10. Waterfall and gray-level display of two linearly converging chirps (a) and two-tone signal (b) using the POCS-designed kernel in Fig. 9. The result is quite good.

constraints of (14), (16), and (17), the realness constraint of (15), and the nonnegativity constraint in (19). Furthermore,

$$\Phi(f,u) = \frac{1}{|f|}\Pi\left(\frac{u}{f}\right)$$

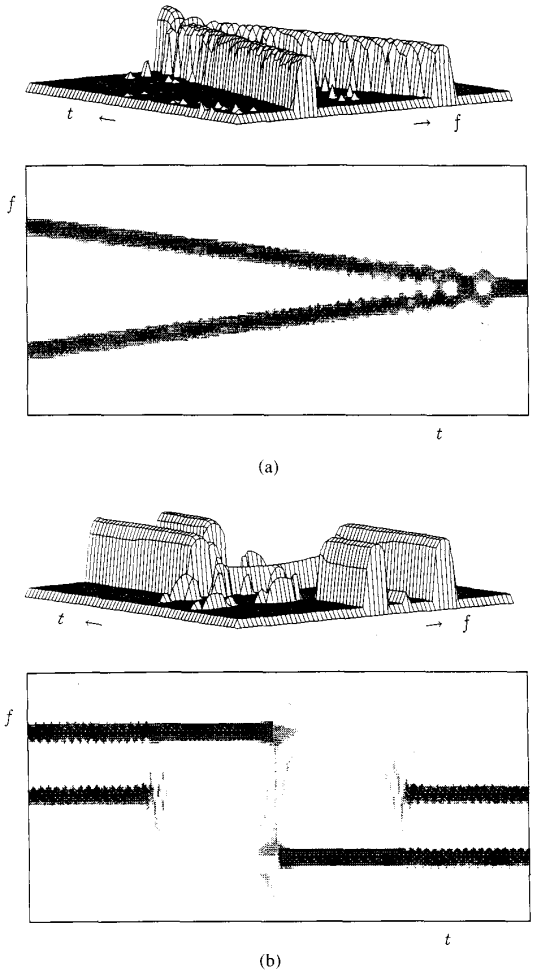

Fig. 11. Use of a cone-shaped kernel with uniform Hanning taper in the τ direction on the two-chirp and two-tone signal. The 35–dB range is the same as in Fig. 10.

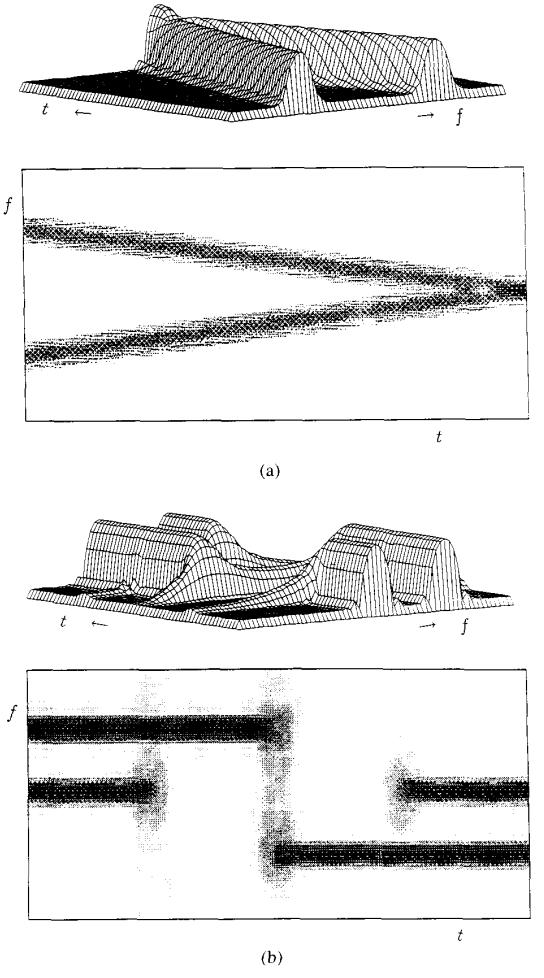

Fig. 12. Spectrogram of the two-chirp and two-tone signal.

satisfies the untruncated bow-tie constraint. Historically, this POCS result first prompted the authors to investigate cone kernels with linear taper [6], [9]. The iterative synthesis of this kernel did not converge. This empirically proves that, for the kernel dimensions used, *there does not exist a kernel that satisfies all of the constraints*. Otherwise, the kernel would have converged. Iteration was stopped on the cone projection. The result is shown in Fig. 7. Application of this kernel to two converging linear chips [8], [10] resulted in the 25 dB waterfall and 30 dB gray level display in Fig. 8(a), and that of the two-tone signal with transition in Fig. 8(b). The distance from floor to peak is 25 dB.

Example 2 removed the marginal constraints. We take the alternating projection between $\mathcal{C}_{3,1} \cap \mathcal{C}_{3,2}$ and $\mathcal{C}_1 \cap \mathcal{C}_9 \cap \mathcal{C}_{10}$. We terminated iteration at the set $\mathcal{C}_1 \cap \mathcal{C}_9$. This resulted is the kernel in Fig. 9. The outcome of the POCS design, smoothed with a Hanning window, was applied to the same linear chirp and two-tone signal problem. The result of the linear chirp and two-tone signal is shown in Fig. 10(a) and (b) using a 35 and 40 dB floor-to-peak range, respectively. Compare this with the cone-shaped kernel result in Fig. 11 with a uniform Hanning window taper in the τ direction. The same 35 dB range is used. For this example, the POCS kernel seems to perform better in terms of interference suppression. To complete the comparison, similarly scaled plots of the spectrogram and Wigner distribution for the same signals are shown, respectively, in Figs. 12 and 13.

VI. Conclusions

We have presented a technique whereby kernels for use in Cohen's class of GTFR's can be synthesized in accordance with desired properties using the method of *projection onto convex sets* (POCS). This technique allows a new perspective on the notion of simultaneously satisfying very different (e.g., time and frequency resolution) constraints. Simulation results show resolution performance better than the spectrogram and bilinear interference reduction, which is much better than the Wigner distribution. The ultimate success of this synthesis methodology is dependent on the suitability of the constraints

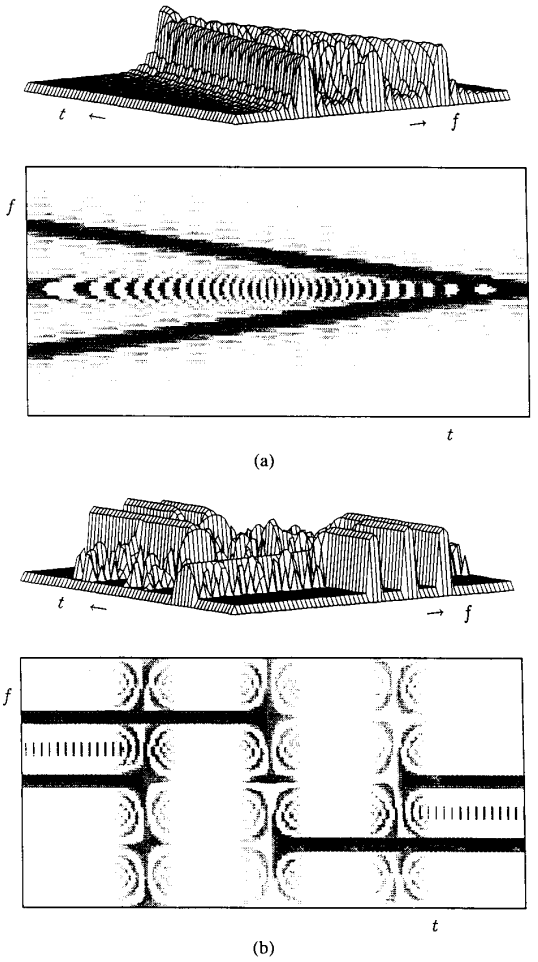

Fig. 13. Wigner distribution of the two-chirp and two-tone signal.

for specific applications. Using POCS, we have empirically proved that, for some kernel dimensions, a kernel does not exist that satisfies all commonly used constraints. Our conjecture is that this nonexistence is always true.

ACKNOWLEDGMENT

The authors express their appreciation to J. W. Pitton and P. Loughlin of the Interactive Systems Design Lab for their input and encouragement.

REFERENCES

[1] R. Koenig, H. Dunn, and L. Lacy, "The sound spectrograph," *J. Acoust. Soc. Amer.*, vol. 18, pp. 19–49, 1946.
[2] O. Rioul and M. Vetterli, "Wavelets and signal processing," *IEEE Signal Processing Mag.*, pp. 14–38, Oct. 1991.
[3] T. A. C. M. Claasen and W. F. G. Mecklenbrauker, "The Wigner distribution, A tool for time–frequency signal analysis, Part 3: Relations with other time-frequency signal transformations," *Philips J. Res.*, vol. 35, pp. 373–389, 1980.
[4] L. Cohen, "Generalized phase-space distribution functions," *J. Math. Phys.*, vol. 7, pp. 781–786, 1966.
[5] ——, "Time–frequency distributions—A review," *Proc. IEEE*, vol. 77, pp. 941–981, 1989.
[6] L. E. Atlas, Y. Zhao, and R. J. Marks, II, "Application of the generalized time–frequency representation to speech signal analysis," in *Proc. IEEE Pacific Rim Conf. Commun., Comput., Signal Processing*, Victoria, B.C., Canada, June 1987, pp. 517–519.
[7] T. A. C. M. Claasen and W. F. G. Mecklenbrauker, "The Wigner distribution, A tool for time–frequency signal analysis, Part 2: Discrete time signals," *Philips J. Res.*, vol. 35, pp. 277–300, 1980.
[8] H. Choi and W. Williams, "Improved time–frequency representation of multicomponent signals using exponential kernels," *IEEE Trans. Acoust., Speech, Signal Processing*, vol. 37, pp. 862–871, 1989.
[9] Y. Zhao, L. E. Atlas, and R. J. Marks, II, "The use of cone-shape kernels for generalized time–frequency representations of nonstationary signals," *IEEE Trans. Acoust., Speech, Signal Processing*, vol. 38, pp. 1084–1091, 1990.
[10] S. Oh and R. J. Marks, II, "Some properties of the generalized time frequency representation with cone shaped kernel," *IEEE Trans. Acoust., Speech, Signal Processing*, vol. 40, July 1992.
[11] P. J. Loughlin, J. W. Pitton, and L. E. Atlas, "Bilinear time–frequency representation: New insights and properties," submitted to *IEEE Trans. Acoust., Speech, Signal Processing*.
[12] L. M. Bregman, "Finding the common point of convex sets by the method of successive projections," *Dokl. Akad. Nauk. USSR*, vol. 162, no. 3, pp. 487–490, 1965.
[13] L. G. Gubin, B. T. Polyak, and E. V. Raik, "The method of projections for finding the common point of convex sets," *USSR Comput. Math. Phys.*, vol. 7, no. 6, pp. 1–24, 1967.
[14] D. C. Youla and H. Webb, "Image restoration by method of convex set projections: Part I—Theory," *IEEE Trans. Med. Imaging*, vol. MI-1, pp. 81–94, 1982.
[15] M. I. Sezan and H. Stark, "Image restoration by method of convex set projections: Part II—Applications and numerical results," *IEEE Trans. Med. Imaging*, vol. MI-1, pp. 95–101, 1982.
[16] S. J. Yen and H. Stark, "Iterative and one-step reconstruction from nonuniform samples by convex projections," *J. Opt. Soc. Amer. A*, vol. 7, pp. 491–499, 1990.
[17] M. R. Civanlar and H. J. Trussel, "Digital signal restoration using fuzzy sets," *IEEE Trans. Acoust., Speech, Signal Processing*, vol. ASSP-34, p. 919, 1986.
[18] R. J. Marks, II, "A class of continuous level associative memory neural nets," *Appl. Opt.*, vol. 26, pp. 2005–2009, 1987.
[19] R. J. Marks, II, S. Oh, and L. E. Atlas, "Alternating projection neural networks," *IEEE Trans. Circuits Syst.*, vol. 36, pp. 846–857, 1989.
[20] M. H. Goldburg and R. J. Marks, II, "Signal synthesis in the presence of an inconsistent set of constraints," *IEEE Trans. Circuits Syst.*, vol. CAS-32, pp. 647–663, 1985.
[21] H. Stark, Ed., *Image Recovery: Theory and Application*. Orlando, FL: Academic, 1987.
[22] D. C. Youla and V. Velasco, "Extensions of a result on the synthesis of signals in the presence of inconsistent constraints," *IEEE Trans. Circuits Syst.*, vol. CAS-33, pp. 465–468, 1986.

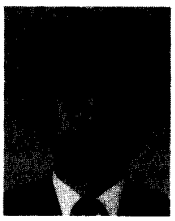

Seho Oh received the B.S. degree in electronics engineering from Seoul National University, the M.S. degree in electrical engineering from Korea Advenced Institute of Science and Technology, Seoul, and the Ph.D. degree, also in electrical engineering, from the University of Washington, Seattle, in 1989.

From 1981 to 1986 he was with the Central Research Laboratory of the Goldstar Company. Currently, he is with Neopath Inc. His research interests are in the areas of signal analysis, generalized time–frequency analysis, artificial neural networks, fuzzy systems, and pattern recognition. He is the coauthor of over 40 archival and proceedings papers and has been issued two U.S. patents.

Robert J. Marks, II (SM'83–F'94) is a Professor in the Department of Electrical Engineering at the University of Washington, Seattle. Dr. Marks is a Fellow of the Optical Society of America. He is the Editor-in-Chief of the IEEE TRANSACTIONS ON NEURAL NETWORKS (1992-present). He was elected to the Board of Governors of the IEEE Circuits and Systems Society (1993-1996) and was the co-founder and first Chair of the *IEEE Circuits and Systems Society Technical Committee on Neural Systems and Applications*. He is the General Chair of the *1995 International Symposium on Circuits and Systems*, Seattle. He is the author of the book *Introduction to Shannon Sampling and Interpolation Theory* (Springer Verlag, 1991) and is editor of the companion volume *Advanced Topics in Shannon Sampling and Interpolation Theory* (Springer Verlag, 1993).

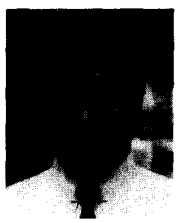

Les E. Atlas received the B.S.E.E. degree from the University of Wisconsin and the M.S. and Ph.D. degrees from Stanford University in 1979 and 1984, respectively. His Ph.D. dissertation was on the design of speech processors for an auditory prosthesis for the profoundly deaf.

He joined the Department of Electrical Engineering, University of Washington, in 1984 and is currently an Associate Professor of Electrical Engineering. He cofounded the Interactive Systems Design Laboratory at the University of Washington, and is currently doing research in acoustic signal processing and recognition, neural network classifiers, and biologically inspired signal processing algorithms and architectures. His research is funded by the Washington Technology Center and Boeing Commercial Airplane Company. He has served as a consultant for many industrial projects, including those with Honeywell Marine Systems, the Boeing Company, and Space Applications.

Dr. Atlas was a 1985 recipient of a National Science Foundation Presidential Young Investigator Award. He was General Chair of the 1992 IEEE Symposium on Time/Scale Analysis and is General Chair of ICASSP '98.